JOURNAL OF THE AMERICAN COLLEGE OF CARDIOLOGY
VOL. 64, NO. 10, 2014

ISSN 0735-1097/$36.00
PUBLISHED BY ELSEVIER INC.
http://dx.doi.org/10.1016/j.jacc.2014.06.1171

In Vivo Imaging of Enhanced Leukocyte Accumulation in Atherosclerotic Lesions in Humans

Fleur M. van der Valk, MD,* Jeffrey Kroon, PhD,† Wouter V. Potters, PhD,‡ Rogier M. Thurlings, MD, PhD,§ Roelof J. Bennink, MD, PhD,‖ Hein J. Verberne, MD, PhD,‖ Aart J. Nederveen, PhD,‡ Max Nieuwdorp, MD, PhD,* Willem J.M. Mulder, PhD,*¶ Zahi A. Fayad, PhD,¶ Jaap D. van Buul, PhD,† Erik S.G. Stroes, MD, PhD*

ABSTRACT

BACKGROUND Understanding how leukocytes impact atherogenesis contributes critically to our concept of atherosclerosis development and the identification of potential therapeutic targets.

OBJECTIVES The study evaluates an in vivo imaging approach to visualize peripheral blood mononuclear cell (PBMC) accumulation in atherosclerotic lesions of cardiovascular (CV) patients using hybrid single-photon emission computed tomography/computed tomography (SPECT/CT).

METHODS At baseline, CV patients and healthy controls underwent ^{18}fluorodeoxyglucose positron emission tomography-computed tomography and magnetic resonance imaging to assess arterial wall inflammation and dimensions, respectively. For in vivo trafficking, autologous PBMCs were isolated, labeled with technetium-99m, and visualized 3, 4.5, and 6 h post-infusion with SPECT/CT.

RESULTS Ten CV patients and 5 healthy controls were included. Patients had an increased arterial wall inflammation (target-to-background ratio [TBR] right carotid 2.00 ± 0.26 in patients vs. 1.51 ± 0.12 in controls; $p = 0.022$) and atherosclerotic burden (normalized wall index 0.52 ± 0.09 in patients vs. 0.33 ± 0.02 in controls; $p = 0.026$). Elevated PBMC accumulation in the arterial wall was observed in patients; for the right carotid, the arterial-wall-to-blood ratio (ABR) 4.5 h post-infusion was 2.13 ± 0.35 in patients versus 1.49 ± 0.40 in controls ($p = 0.038$). In patients, the ABR correlated with the TBR of the corresponding vessel (for the right carotid: $r = 0.88$; $p < 0.001$).

CONCLUSIONS PBMC accumulation is markedly enhanced in patients with advanced atherosclerotic lesions and correlates with disease severity. This study provides a noninvasive imaging tool to validate the development and implementation of interventions targeting leukocytes in atherosclerosis. (J Am Coll Cardiol 2014;64:1019–29) © 2014 by the American College of Cardiology Foundation.

Atherosclerosis remains subclinical over decades prior to the acute onset of major cardiovascular (CV) events (1). Leukocytes are key cellular effectors in atherosclerosis, mediating proinflammatory processes throughout all stages of atherogenesis (2). Following the increased expression of adhesion molecules by activated endothelial cells (3), monocytes—among other leukocytes—are

From the *Department of Vascular Medicine, Academic Medical Center, Amsterdam, the Netherlands; †Department of Molecular Cell Biology, Sanquin Research and Landsteiner Laboratory, Academic Medical Center, Amsterdam, the Netherlands; ‡Department of Radiology, Academic Medical Center, Amsterdam, the Netherlands; §Department of Internal Medicine, Academic Medical Center, Amsterdam, the Netherlands; ‖Department of Nuclear Medicine, Academic Medical Center, Amsterdam, the Netherlands; and the ¶Translational and Molecular Imaging Institute, Icahn School of Medicine at Mount Sinai, New York, New York. This study was supported in part by a research grant from Bristol-Myers Squibb (CVC202-009). The authors acknowledge the support from the Netherlands CardioVascular Research Initiative: the Dutch Heart Foundation, Dutch Federation of University Medical Centres, the Netherlands Organization for Health Research and Development, and the Royal Netherlands Academy of Sciences (CVON 2011/B019 GENIUS). The study was supported by a Dutch Heart Foundation grant (CVON-2011/B-019: GENIUS), a Dutch Technology Foundation grant (STW CARISMA 11629), and an educational grant of BMS (New York, New York; study ID: CV197-006). All authors have reported that they have no relationships relevant to the contents of this paper to disclose.
Listen to this manuscript's audio summary by *JACC* Editor-in-Chief Dr. Valentin Fuster.
You can also listen to this issue's audio summary by *JACC* Editor-in-Chief Dr. Valentin Fuster.

Manuscript received May 6, 2014; revised manuscript received May 30, 2014, accepted June 10, 2014.

JACC VOL. 64, NO. 10, 2014
SEPTEMBER 9, 2014:1019–29

ABBREVIATIONS AND ACRONYMS

^{99m}Tc = technetium 99m

ABR = arterial-wall-to-blood ratio

CV = cardiovascular

FDG-PET/CT = ^{18}fluorodeoxyglucose positron emission tomography/computed tomography

HMPAO = hexamethylpropylene amine oxime

MRI = magnetic resonance imaging

MWA = mean wall area

MWT = mean wall thickness

NWI = normalized wall index

PBMC = peripheral blood mononuclear cell

ROI = region of interest

SPECT = single-photon emission computed tomography/computed tomography

TBR = target-to-background ratio

recruited to these early atherosclerotic lesions (4), leading to the initiation or progression of atherogenesis (5). In support of a causal role of increased monocyte influx in atherogenesis, attenuation of monocyte recruitment by pharmacological interventions has been shown to attenuate atherosclerosis in experimental models (6–9). Although fewer in number, T cells also contribute to the inflammatory response (10,11).

SEE PAGE 1030

In humans, a high white blood cell count correlates with the risk of a CV event (12,13), suggesting that elevated levels of circulating leukocytes represent an expanded pool of inflammatory cells promoting disease progression. Similarly, risk factors for atherosclerosis have been associated with an increased activation state of monocytes (14–16). Nonetheless, data on the in vivo dynamics of leukocytes in human atherogenesis are scarce.

Several dual-modality integrated imaging methods have emerged to quantify the inflammatory activity within atherosclerotic lesions, including ^{18}fluorodeoxyglucose positron emission tomography/computed tomography (PET/CT) to assess arterial wall metabolic activity as an index of macrophage content (17) and iron oxide-enhanced magnetic resonance imaging (MRI) to quantify plaque macrophages (18). These techniques, however, lack the ability to address the in vivo dynamics of leukocytes.

Understanding how leukocytes participate in atherogenesis remains pivotal to our understanding how atherosclerotic lesions develop, and could aid in identifying potential therapeutic targets. In the present study, we used single-photon emission computed tomography (SPECT) and transmission computed tomography (CT) performed simultaneously via a hybrid imaging device (SPECT/CT) as a noninvasive imaging technique capable of visualizing the migratory behavior of technetium-99m (^{99m}Tc)-labeled immune cells in humans (19). In patients with atherosclerosis, we evaluated hybrid SPECT/CT imaging to assess the accumulation of circulating peripheral blood mononuclear cells (PBMC) in atherosclerotic plaques in vivo.

METHODS

STUDY PARTICIPANTS AND PROCEDURES. In this single-center imaging study, patients with atherosclerotic CV disease, age ≥18 years of either sex, were recruited at our outpatient clinic using the following inclusion criteria: documented history of myocardial infarction, transient ischemic attack or stroke, and stable medication for at least 6 weeks prior to study participation. Exclusion criteria included ongoing inflammatory diseases, use of systemic anti-inflammatory drugs and major hepatic (aspartate aminotransferase/alanine aminotransferase >2 times the upper limit of normal) dysfunction. Healthy controls were matched to the patients for age, sex, and body mass index, and were ineligible in case of a medical history of CV disease. Each subject provided written informed consent. The study was approved by the local institutional review board and conducted according to the principles of the International Conference on Harmonisation-Good Clinical Practice guidelines. In all subjects, we performed baseline laboratory tests, including lipid and inflammatory profile, and vascular imaging, consisting of FDG-PET/CT, MRI, and SPECT/CT for visualizing PBMC accumulation.

PBMC ISOLATION AND LABELING. In each subject, venous blood (120 ml) was drawn via an 18G intravenous (IV) line into 4 syringes (30 ml per syringe) containing 5 ml acid citrate dextrose (disodiumcitrate 3%/glucose 2.5%) and 5 ml EloHAES 6% (Fresenius Kabi, Zeist, the Netherlands). On average 20×10^6 PBMC were isolated using Ficoll-Paque Premium ($d = 1.077$ g/ml) density gradient centrifugation (GE Healthcare, Chalfont St. Giles, Buckinghamshire, United Kingdom). The radiolabel technetium 99m-hexamethylpropylene amine oxime (^{99m}Tc-HMPAO) was freshly prepared using a ready-for-labeling kit (Ceretec, GE Healthcare, Eindhoven, the Netherlands). Directly after preparation, PBMCs were incubated with ^{99m}Tc-HMPAO (1,100 MBq/2 ml). Under these conditions, uptake of ^{99m}Tc-HMPAO intracellular is reached before the onset of its decomposition into the constituents, which are unable to cross the cellular membrane, resulting in the cellular trapping of the radiotracer (20). Excess of extracellular ^{99m}Tc-HMPAO was diluted and removed after centrifugation. Finally, radiolabeled autologous PBMC (200 MBq) were resuspended in 3 ml EloHAES 6 prior to reinfusion.

EFFECTS OF PBMC ISOLATION AND LABELING. PBMC migration and accumulation is a multistep process mediated by other adhesion molecules. To assure plausible in vivo behavior of autologous labeled PBMC, we assessed PBMC behavior in terms of migratory and adhesive capacity via flow cytometry and an in vitro transendothelial migration assay (21) after isolation and labeling procedures. For flow cytometry, PBMC were incubated with antibodies

(PECy7-CD14, APC-Cy7-CD16, PerCpCy5.5-HLA-DR, APC-CD11c, APC-CD18 1:50; all BD Biosciences, San Jose, California) for 15 min and washed with saline. Red blood cells were lysed with BD FACSTM-lysis solution (BD Biosciences, California). Samples were analyzed by flow cytometry using an FACSCalibur (Becton Dickinson, Franklin Lakes, New Jersey). For analysis, monocytes were identified by CD14, CD16, and HLA-DR expression (22), and the integrins CD11c and CD18 were used as markers of adhesive capacity (23). For the transendothelial migration assay, primary human arterial endothelial cells (Lonza, Baltimore, MD) were cultured on an fibronectin-coated glass cover and stimulated overnight with tumor necrosis factor-α (10 ng/ml). PBMC at a concentration of 1×10^6 cells/ml were added to the human arterial endothelial cells monolayer for 30 min at 37°C and then fixed with 3.7% formaldehyde (Sigma-Aldrich, Zwijndrecht, the Netherlands). After fixation, multiple images were recorded with a Zeiss Axiovert 200 microscope (Plan-apochromat 10×/0.45 M27 Zeiss-objective; Carl Zeiss, Jena, Germany) and analyzed using ImageJ software (NIH, ImageJ.net, US; version 1.48t/March 28, 2014).

VASCULAR IMAGING, FDG-PET/CT IMAGING. FDG-PET/CT scans were performed on a Gemini time-of-flight multidetector PET/CT scanner (Philips, Best, the Netherlands) as previously described (24). In brief, subjects fasted for at least 6 h prior to infusion of 200 MBq of FDG (5.5 mCi). After 90 min, subjects underwent PET/CT imaging initiated with a low-dose CT for attenuation correction and anatomic co-registration. PET/CT images stripped of metadata were analyzed by 1 blinded experienced reader (F.M.) using OsiriX (Geneva, Switzerland). FDG uptake was assessed in the arterial wall of the ascending aorta and left and right carotid arteries. In each artery, 5 regions of interest (ROIs) were drawn, delineating the arterial wall. Maximum standardized uptake values were averaged for each artery. The target-to-background ratio (TBR) was calculated from the ratio of maximal arterial standardized uptake values and mean venous background activity within the superior caval vein (correction for aorta) and the jugular vein (correction for carotids) (24).

Magnetic resonance images were obtained with a 3.0-T whole-body scanner (Ingenia, Philips Medical Systems, Best, the Netherlands), using an 8-channel carotid artery coil (Shanghai Chenguang Medical Technologies, Shanghai, China). One blinded reader performed image analysis using semiautomated measurement software (VesselMass, Leiden, the Netherlands). Mean wall thickness (MWT), mean wall area (MWA), and the normalized wall index (NWI = mean wall area/outer wall area) were calculated (25).

TABLE 1 Baseline Characteristics of Subjects

Characteristic	CV Patients (n = 10)	Control Subjects (n = 5)	p Value
Age, yrs	56 ± 7	50 ± 3	NS
Male	7 (70)	4 (80)	NS
BMI, kg/m^2	28 ± 5	28 ± 6	NS
SBP, mm Hg	132 ± 12	133 ± 10	NS
DBP, mm Hg	82 ± 8	82 ± 2	NS
Active smoking (yes), %	3 (30)	0 (0)	NS
Statin use (yes), %	9 (90)	0 (0)	0.03
Tot chol, mmol/l	5.26 ± 2.26	5.04 ± 0.19	NS
LDLc, mmol/l	3.30 ± 2.24	3.08 ± 0.21	NS
HDLc, mmol/l	1.37 ± 0.47	1.47 ± 0.41	NS
WBC, 10E9/l	6.93 ± 2.00	5.42 ± 0.95	NS
Monocytes, 10E9/l	0.52 ± 0.16	0.35 ± 0.06	0.01
CRP, mg/l	0.65 (0.30-10.70)	1.90 (0.30-3.60)	NS

Values are mean ± SD, n (%) or total range.

BMI = body mass index; CRP = C-reactive protein; CV = cardiovascular; DBP = diastolic blood pressure; HDLc = high-density lipoprotein cholesterol; LDLc = low-density lipoprotein cholesterol; NS = not significant; SBP = systolic blood pressure; Tot chol = total cholesterol; WBC = white blood cells.

PBMC TRAFFICKING BY SPECT/CT. All subjects underwent SPECT imaging (Symbia T16, Siemens, Erlangen, Germany) with low-dose, non-contrast-enhanced CT for attenuation correction and anatomic coregistration, at 3, 4.5, and 6 h post-infusion of 200 MBq ^{99m}Tc-HMPAO labeled autologous PBMCs. SPECT/CT images were analyzed using OsiriX (Geneva, Switzerland) and MeVisLab (Bremen, Germany). Two readers, who were offered datasets stripped of metadata on subject history and time post-infusion, analyzed the SPECT images twice. Accumulation of labeled PBMCs in the arterial wall was quantified in the ascending aorta and left and right carotid arteries using anatomical landmarks to ensure analysis of the same arterial segments over time: for the carotids, 1 slice caudal to the bifurcation; for the ascending aorta 1 slice cranial to the joining of the pulmonary arteries. In each artery, 5 ROIs were drawn, delineating the arterial wall. The maximum counts in the arterial wall ROIs were averaged over each artery to derive an averaged maximum arterial count. To correct for the ^{99m}Tc activity in the blood, 5 venous ROIs were drawn within the superior caval (correction for aorta) and the jugular vein (correction for carotids) to obtain the averaged mean counts of the blood. The values provided in the present paper represent the ratio of the averaged maximum counts of the artery divided by the averaged mean counts in the blood. These values are reported as the arterial-wall-to-blood ratio (ABR).

TABLE 2 Baseline Vascular Imaging Parameters

Imaging Parameter	CV Patients (n = 10)	Control Subjects (n = 5)	p Value
NWI	0.52 ± 0.09	0.33 ± 0.02	0.026
MWT, mm	1.54 ± 0.54	0.64 ± 0.03	0.046
MWA, mm^2	40.38 ± 18.15	14.32 ± 1.62	0.029
TBR left carotid	1.77 ± 0.27	1.34 ± 0.16	0.050
TBR right carotid	2.00 ± 0.26	1.51 ± 0.12	0.022
TBR aorta	2.84 ± 0.69	1.90 ± 0.14	0.003

Values are mean ± SD.

MWA = mean wall area; MWT = mean wall thickness; NWI = normalized wall index; TBR = target-to-background ratio.

STATISTICAL ANALYSIS. Baseline values and distributional characteristics are shown as mean ± SD, number (frequency), or median (min-max). Independent samples *t* test, Mann-Whitney *U* tests, and chi-square tests were used to assess differences between patients and controls. To assess the differences over time in PBMC accumulation, a paired *t* test or Wilcoxon signed rank test was applied. The following correlations were assessed using Pearson's or Spearman's correlation coefficient: 1) ABR at 4.5 and 6 h with the TBR; 2) carotid ABR at 4.5 and 6 h with carotid NWI, MWT, and MWA; and 3) ABR of the index vessel (highest ABR of either the left/right carotid or aorta) at 4.5 and 6 h to nonimaging parameters. To assess interobserver variability, 2 readers analyzed the SPECT/CT images and calculated intraclass correlation coefficients with 95% confidence intervals. A 2-sided p value <0.05 was considered statistically significant. All data were analyzed using Prism version 5.0 (GraphPad software, La Jolla, California) and SPSS version 19.0 (SPSS Inc., Chicago, Illinois).

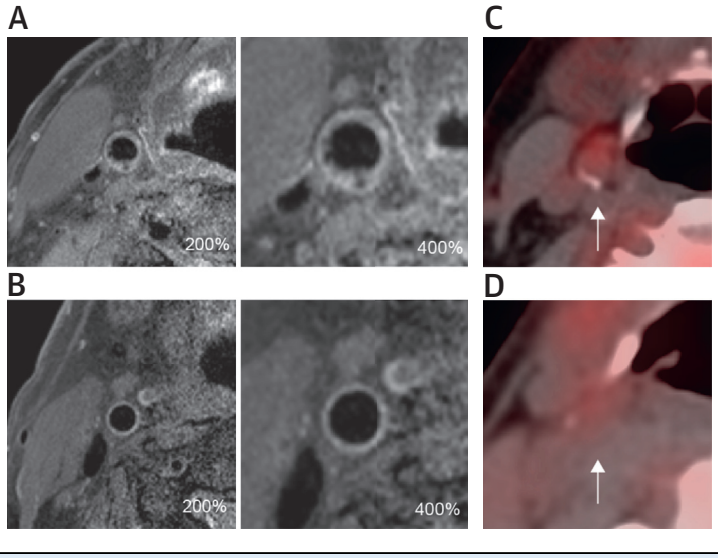

FIGURE 1 MRI and PET/CT Images of the Carotid Artery at Baseline

Representative cross-sectional magnetic resonance imaging (MRI) images of the right common carotid artery of **(A)** a CV patient and **(B)** a healthy control are shown, zoomed in 200% and 400%. Corresponding cross-sectional fused positron emission tomography/computed tomography (PET/CT) images of the right common carotid **(white arrow)** are shown of a cardiovascular (CV) patient **(C)** and healthy control **(D)**.

RESULTS

BASELINE CHARACTERISTICS. In total, 10 CV patients and 5 healthy control subjects were included (Table 1). The groups were balanced for age and sex. Cardiovascular patients had a history of myocardial infarction (n = 5), transient ischemic attack (n = 2), or ischemic stroke (n = 3). At baseline, traditional CV risk factors did not significantly differ between groups (Table 1). Almost all CV patients (90%) were on stable statin therapy. Baseline laboratory analysis revealed no differences in lipid profiles between CV patients and controls (Table 1). Neither white blood cell count nor C-reactive protein differed significantly, although CV patients did exhibit a higher level of circulating monocytes compared to control subjects (0.52 ± 0.16 × 10^9/l in patients versus 0.35 ± 0.06 × 10^9/l in controls; p = 0.013).

Baseline vascular imaging confirmed that the CV patients included in the study were characterized by advanced atherosclerotic lesions (Table 2). First, MRIs showed an increased atherosclerotic burden in the CV patients compared to healthy controls: 1) MWT was increased (1.54 ± 0.54 mm vs. 0.64 ± 0.03 mm; p = 0.046); 2) MWA was enlarged (40.38 ± 18.15 mm^2 vs. 14.32 ± 1.62 mm^2; p = 0.029); and, in line, 3) NWI was higher (0.52 ± 0.09 vs. 0.33 ± 0.02; p = 0.026). Second, PET/CT imaging corroborated an enhanced TBR of the right carotid artery in CV patients (TBR_{max} 2.00 ± 0.26) versus controls (TBR_{max} 1.51 ± 0.12; p = 0.022) (26). Comparable differences in TBR in patients versus controls were observed in the left carotid and aorta (Table 2). Figure 1 shows representative cross-sectional MRI and PET/CT images of the right carotid artery, illustrating a CV patient's atherosclerotic burden.

EFFECT OF ISOLATION AND LABELING. Prior to evaluating the in vivo behavior of PBMCS, we first assessed the effects of our isolation and labeling procedures in terms of migratory and adhesive capacity via flow cytometry and an in vitro transendothelial migration assay. First, the differentiation

of monocytes in their proinflammatory, intermediate, and anti-inflammatory subsets (13) was not affected by the isolation and labeling procedures (for monocyte 1: 90.67% prior and 90.63% after labeling procedures; p = NS) (Figure 2A). Second, the expression of adhesion markers also did not change significantly. Delta mean fluorescence intensity of CD11c was 316 ± 2 prior to labeling versus 304 ± 8 after labeling (p = NS) and delta mean fluorescence intensity of CD18 was 618 ± 18 prior to labeling versus 586 ± 14 after (p = NS) (Figure 2B). Third, the TEM assay corroborated that the labeling procedure did not affect the capacity of monocytes to cross the endothelial monolayer (prior to labeling 36 ± 12 vs. 25 ± 3 cells/mm^2 after labeling, p = NS) (Figure 2C).

IMAGING PBMC ACCUMULATION IN ATHEROSCLEROTIC LESIONS WITH SPECT/CT. In all subjects, we performed SPECT/CT imaging 3, 4.5, and 6 h post-infusion of radiolabeled autologous PBMCS. Prior to assessing differences between groups, interobserver agreement for the SPECT/CT images reading demonstrated proper intraclass correlation coefficient of 0.87 with a narrow 95% confidence interval (0.75 to 0.96).

At the first time point (3 h post infusion), the ABR, representing PBMC accumulation, was higher in CV patients but not significantly so compared to controls (ABR for aorta 3.68 ± 1.23 vs. 2.93 ± 1.37; p = NS) (Figure 3A). In contrast, at 4.5 h and 6 h ABR stood significantly higher in patients compared to controls. For the ascending aorta, the ABR at 4.5 h was 5.41 ± 2.29 in patients versus 2.59 ± 0.90 in controls (p = 0.013), increasing at 6 h to 8.19 ± 4.49 in patients versus 2.80 ± 1.19 in controls (p = 0.012) (Figure 3A). Figure 4 depicts illustrative cross-sectional SPECT/CT images of the ascending aorta at 3 anatomic levels at 4.5 h following infusion, showing an enhanced PBMC accumulation in a CV patient versus a control subject. Corresponding results were found when analyzing the left and right carotid artery (Figures 3B and 3C). Table 3 contains an overview of the PBMC accumulation at the 3 time points for every artery in patients versus controls.

From 3 to 6 h, the rate of PBMC accumulation increased significantly in patients, whereas there was no change in ABR over time in control subjects (change in ABR from 3 to 6 h 4.50 ± 3.63 in patients vs. -0.13 ± 0.25 in controls; p = 0.009) (Figure 3D). Figures 5 and 6 include representative SPECT/CT images in which the ascending aorta was segmented out and PBMC accumulation was visualized over time, showing the increase in ABR from time points 3 to 4.5 h in a typical CV patient versus no change in a control subject.

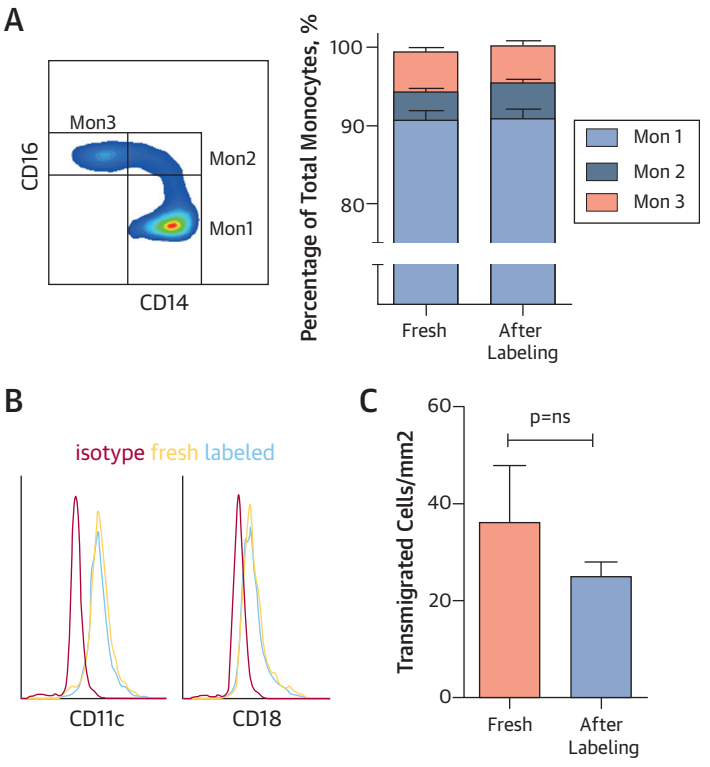

FIGURE 2 PBMC Behavior After Isolation and Labeling

Flow cytometry analysis showed that labeling procedures did not significantly alter monocyte subset division **(A)** and did not significantly change the expression of adhesion markers CD11c and CD18 **(B)**. Transendothelial migration assays corroborated that the labeling procedure did not significantly change their migratory capability **(C)**. Mon = monocyte; PBMC = peripheral blood mononuclear cell.

CORRELATION BETWEEN PBMC ACCUMULATION AND DISEASE SEVERITY. In patients, the ABR (PBMC accumulation) as measured with SPECT/CT correlated with the TBR (arterial wall inflammation) of the corresponding vessel assessed via PET/CT. For the right carotid, both the ABR at 4.5 and at 6 h correlated with the right carotid artery TBR (r = 0.76, p = 0.007; and r = 0.88, p = 0.014, respectively). Figure 3E shows the correlation of ABR at 4.5 h following infusion with the TBR of the right carotid. Moreover, the change in ABR from 3 to 6 h in the right carotid artery also correlated with TBR (r = 0.79, p = 0.011). Similar correlations were seen in the left carotid artery and ascending aorta; however, MRI revealed no significant correlations between ABR and arterial wall dimensions (Table 4). Besides, no correlation between circulating immune cells and PBMC accumulation was observed (for circulating monocytes: r = 0.15, p = NS), whereas the level of C-reactive protein did correlate with PBMC

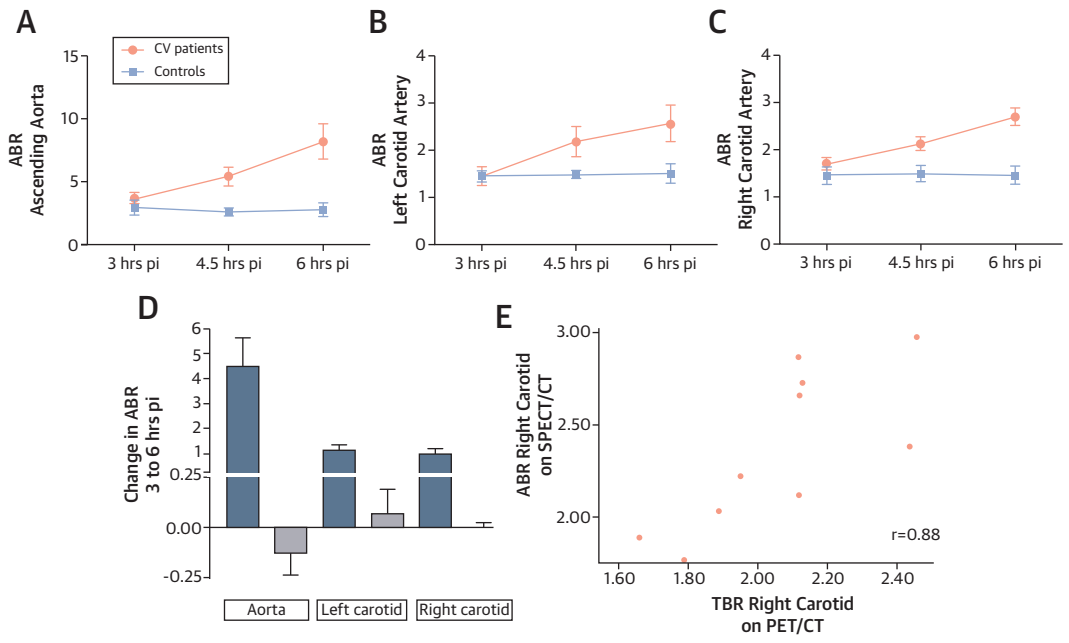

FIGURE 3 ABR of PBMC Accumulation on SPECT/CT

Line graphs showing increased signal intensities in cardiovascular (CV) patients versus control subjects in 3 time points at 3 different anatomical locations: ascending aorta **(A)**, left carotid artery **(B)**, and right carotid artery **(C)**. The bar graphs indicate the change in signal intensity from 3 to 6 h post-infusion, showing a marked increase over time in patients versus no significant changes in control subjects **(D)**. Shown here for the right carotid artery, the arterial-wall-to-blood ratio (ABR) at 4.5 h correlated with the target-to-background ratio (TBR) assessed via PET/CT **(E)**. SPECT/CT = single-photon emission computed tomography/computed tomography; other abbreviation as in Figure 2.

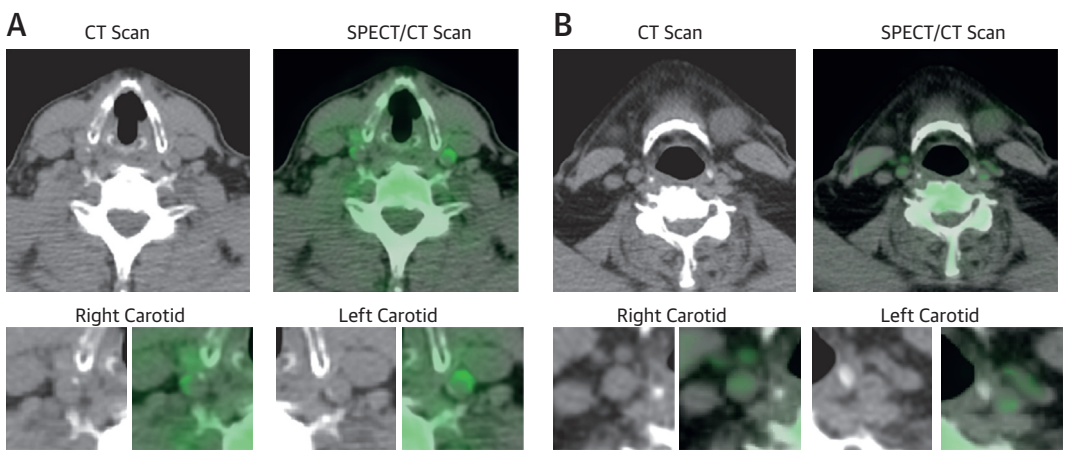

FIGURE 4 SPECT/CT of the Carotid Arteries in a CV Patient and Control

Representative cross-sectional single-photon emission computed tomography/computed tomography (SPECT/CT) images at 4.5 h of the neck region, and zoomed in for the left and right carotid artery of a cardiovascular (CV) patient **(A)** and a healthy control **(B)**.

accumulation in the arterial wall ($r = 0.76$, $p = 0.030$). The classic CV risk factors, total cholesterol and low-density lipoprotein cholesterol, also correlated to the change in ABR over time ($r = 0.72$, $p = 0.044$; $r = 0.77$, $p = 0.027$, respectively).

TABLE 3 ABR and ΔABR in Patients and Controls

	Time Post-Infusion, h	CV Patients (n = 10)	Control Subjects (n = 5)	p Value
Left carotid	3	1.44 ± 0.65	1.44 ± 0.24	0.981
	4.5	2.18 ± 1.01	1.47 ± 0.23	0.050
	6	2.57 ± 1.21	1.50 ± 0.45	0.044
	ΔABR	1.13 ± 0.72	0.07 ± 0.27	0.004
Right carotid	3	1.70 ± 0.41	1.45 ± 0.41	0.359
	4.5	2.13 ± 0.35	1.49 ± 0.40	0.038
	6	2.69 ± 0.61	1.45 ± 0.43	0.003
	ΔABR	1.00 ± 0.53	0.00 ± 0.05	0.001
Aorta	3	3.68 ± 1.23	2.93 ± 1.37	0.390
	4.5	5.41 ± 2.29	2.59 ± 0.90	0.013
	6	8.19 ± 4.49	2.80 ± 1.19	0.012
	ΔABR	4.50 ± 3.63	−0.13 ± 0.25	0.009

Values are mean ± SD.
ABR = arterial-wall-to-blood ratio; CV = cardiovascular.

DISCUSSION

In the present study, we demonstrate that in vivo hybrid SPECT/CT imaging can detect PBMC accumulation in the arterial wall, showing a marked increase in PBMC accumulation in patients with atherosclerotic disease with no corresponding accumulation in control subjects. The degree of PBMC accumulation in the arterial wall correlated to the degree of arterial wall inflammation as assessed with PET/CT. Moreover, PBMC accumulation correlated with the established CV risk factors low-density lipoprotein cholesterol and C-reactive protein. These preliminary data lend further support to strategies aimed at attenuating leukocyte recruitment as a therapeutic target in CV patients.

LEUKOCYTE RECRUITMENT AND ACCUMULATION. Dissecting how leukocytes participate in atherogenesis is challenging due to their dynamics and functional heterogeneity (4). In the present study, we observed marked and rapid PBMC accumulation in atherosclerotic lesions in humans. Support for this finding comes from several experimental models demonstrating active monocyte accumulation in the course of atherogenesis (27,28), which was proportional to the atherosclerotic burden (29). Notwithstanding the presence of active leukocyte recruitment in atherogenesis (30), the biological fate of extravasated leukocytes remains less defined (31). In early lesions, leukocytes infiltrate the arterial wall, giving rise

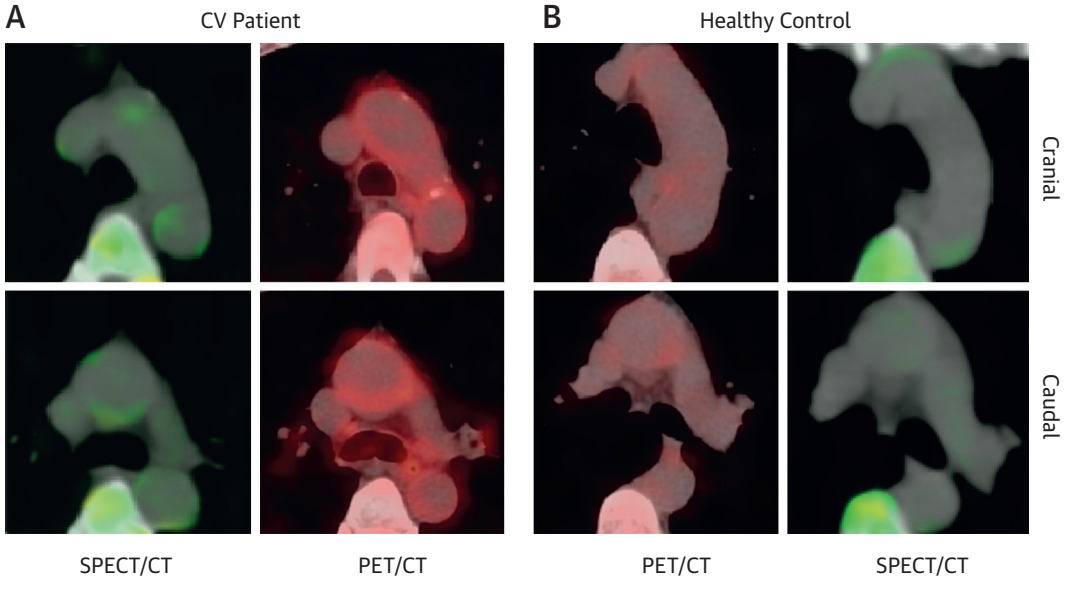

FIGURE 5 SPECT/CT and PET/CT Images of the Ascending Aorta

Representative cross-sectional SPECT/CT at 4.5 h and PET/CT images of the ascending aorta at 2 levels of a CV patient **(A)** and a healthy control **(B)** are shown, indicating the significant differences in both PBMC accumulation (ABR) as arterial wall inflammation (TBR) between the CV patient and the control subject, and the correlation between ABR and TBR. Abbreviations as in Figures 1, 2, and 4.

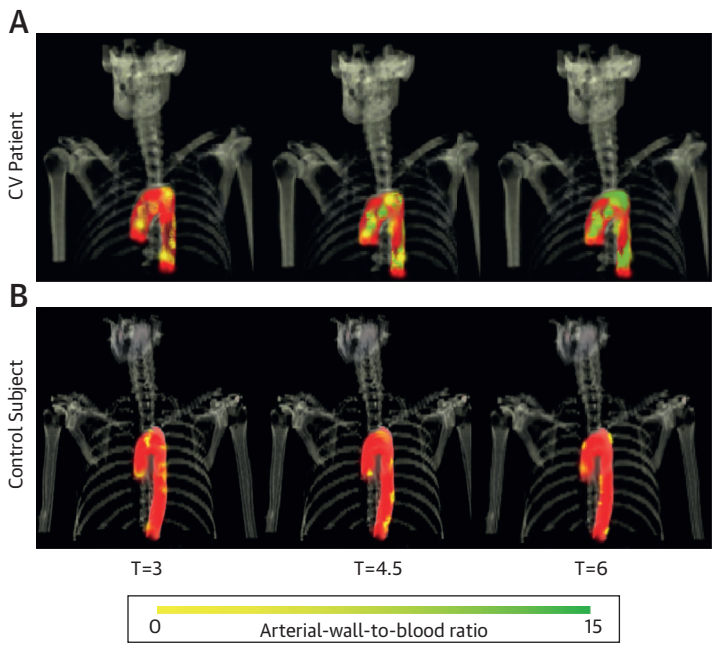

FIGURE 6 PBMC Accumulation Over Time Via SPECT/CT

Single-photon emission computed tomography/computed tomography (SPECT/CT) images, in which the ascending aorta was segmented out (shown in **red**) to visualize the significant increase in peripheral blood mononuclear cell (PBMC) accumulation from 3 to 4.5 and 6 h post-infusion in the cardiovascular (CV) patient **(A)** versus no increase in the control subject **(B)**.

to the initial pool of tissue descendants including macrophages and T cells (32). In advanced lesions, research suggests the contribution of freshly infiltrated monocytes to the macrophage content to be less significant (33), following the observation that local proliferation may in fact be the major source of lesional macrophages in experimental atherosclerosis (34). The latter, however, does not indemnify the importance of leukocyte recruitment in advanced atherosclerosis (35). Integrating the data suggests that in early lesions, freshly recruited cells contribute to the subintimal inflammatory cell burden, whereas in more advanced lesions continuous leukocyte influx propagates inflammation, eventually promoting plaque vulnerability (5,36) and risk of a (recurrent) CV event (37). In fact, circulating leukocytes of CV patients already exhibit a distinct functional phenotype, which is proportional to the CV event rate (12,13) and potentially mediated via alterations of the epigenome (14,16).

TABLE 4 Correlation Between ABR and Read-Out Parameters of PET/CT and MRI

	ABR 4.5-h Post-Infusion	p Value	ABR 6-h Post-Infusion	p Value	ΔABR 3–6-h Post-Infusion	p Value
PET/CT						
TBR left carotid	0.67	0.049	0.69	0.042	0.78	0.012
TBR right carotid	0.76	0.007	0.881	<0.001	0.79	0.011
TBR aorta	0.72	0.028	0.52	0.150	0.53	0.142
MRI						
NWI	0.70	0.125	0.74	0.09	0.52	0.292
MWT	0.67	0.145	0.72	0.107	0.51	0.303
MWA	0.68	0.140	0.72	0.106	0.51	0.299

ABR = arterial-wall-to-blood ratio; MRI = magnetic resonance imaging; PET/CT = positron emission tomography/computed tomography; other abbreviations as in Table 2.

CORRELATIONS WITH PBMC ACCUMULATION. We observed several correlations between CV risk factors and PBMC accumulation. First, PBMC accumulation correlated with FDG uptake assessed with PET/CT. In turn, arterial wall FDG uptake has been correlated to plaque macrophage content (24,38) and risk of a recurrent CV event (37). Second, PBMC accumulation also correlated to the level of plasma C-reactive protein, a marker of systemic inflammation also indicative of CV risk (39).

Another correlation was observed between PBMC accumulation and low-density lipoprotein cholesterol, which may have several explanations. Patients with higher low-density lipoprotein cholesterol may have a higher atherosclerotic disease burden and hence higher PBMC influx. However, we did not observe a correlation between PBMC accumulation and arterial wall dimensions assessed with MRI. Alternatively, higher levels of circulating low-density lipoprotein cholesterol may lead to the activation of leukocytes and increased arterial wall PBMC influx. In support, monocytes in hyperlipidemic conditions have an increased expression of adhesion makers (40) and are more avidly recruited to the atherosclerotic lesion (28,29). Overall, the data imply that increased PBMC recruitment is involved in disease progression in patients with advanced atherosclerotic lesions.

LIMITATIONS OF SPECT/CT. The present approach of PBMC imaging with SPECT/CT merits some considerations. A confounding variable in our findings is the potential for in vitro PBMC activation by the labeling procedures. However, flow cytometry and transendothelial migration assays did not show PBMC activation related to adhesive capacity of the labeling procedures. Moreover, the infusion of labeled PBMC was also not associated with an increased ABR in healthy controls. Additionally, the current technique could be refined by applying more sophisticated isolation procedures allowing future investigations to specifically study subpopulations of leukocytes. Extensive ex vivo procedures, however, could change the in vivo behavior of the leukocytes prior to re-infusion. Our current approach lacks the ability to quantify leukokinetics in terms of continuous

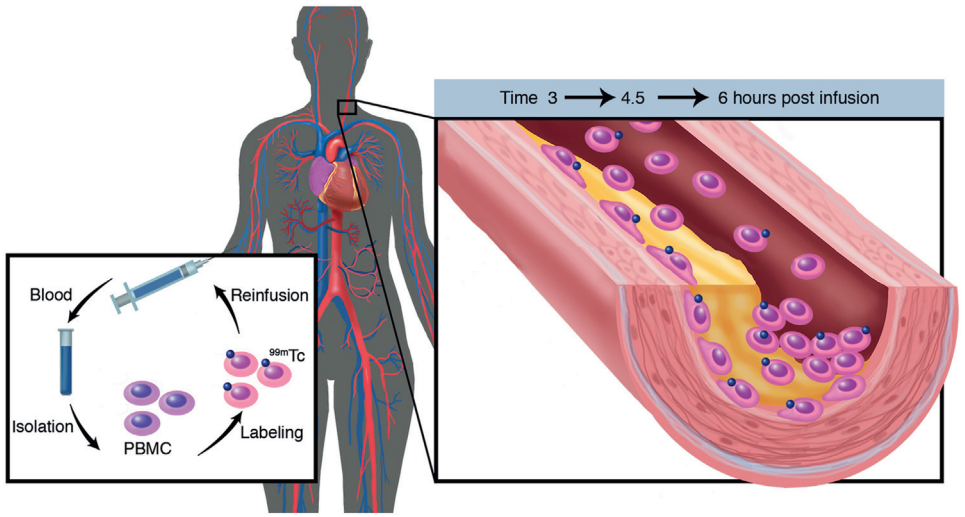

CENTRAL ILLUSTRATION **Imaging of Leukocyte Accumulation in Atherosclerosis**

Reinfusion of autologous, labeled leukocytes was applied to assess leukocyte accumulation in the arterial wall using serial single-photon emission computed tomography/computed tomography imaging in humans. Accumulation was found to be markedly enhanced in patients with advanced atherosclerotic lesions. PBMC = peripheral blood mononuclear cell.

recruitment, influx, differentiation and efflux, or apoptosis. If recruited cells rapidly undergo apoptosis, this may lead to radiotracer loss and underestimation of the SPECT signal. Finally, we performed 3 SPECT scans and a low-dose CT for attenuation correction and co-registration. Increasing the CT dose or infusing a contrast agent could provide greater anatomic and radiotracer signal detail, but with a higher radiation burden. Moreover, we used ^{99m}Tc as a radiotracer, which has a half-life of 6 h, thereby allowing rapid data collection and limiting radiation exposure. Applying a radiotracer with a longer half-life, such as ^{111}Indium (half-life 2.8 days) for SPECT or a positron emitter like ^{89}Zirconium (half-life 3.3 days) for PET, would enable investigators to study leukocyte trafficking for longer periods of time. However, this would expose the patient to greater radiation doses.

CLINICAL IMPLICATIONS. In an attempt to silence plaque's inflammatory activity, therapeutic interventions targeting leukocytes could act at multiple levels; for instance, modulation of circulating leukocytes, reduction of adhesion, and changes in differentiation or emigration of leukocytes. Regarding recruitment and adhesion, alterations in the expression of the adhesion molecules (41), chemotactic factors (6-9) or combined inhibition strategies (42) all favorably affect plaque size and progression in experimental models. To date, however, interventions in these pathways in patients have not shown a clinical benefit (43,44). Our current observation of rapid PBMC accumulation in patients with advanced atherosclerosis (**Central Illustration**) lends further support to the targeting of leukocytes as a promising strategy against atherogenesis (45). Our presented approach of in vivo leukocyte trafficking with SPECT/CT imaging could be applied to study mechanistic hypotheses in humans, as well as provide early insights in the efficacy of interventions targeting leukocytes in CV patients.

CONCLUSIONS

We present an imaging approach to visualize leukocyte migration to atherosclerosis in humans and demonstrate an increased PBMC accumulation in patients with advanced atherosclerosis. Current data support efforts to develop intervention strategies targeting leukocytes to modulate the inflammatory processes in atherosclerosis.

ACKNOWLEDGMENTS The authors would like to thank G.M. Dallinga-Thie for lab advice and W.M. de Jong for assistance with SPECT/CT.

REPRINT REQUESTS AND CORRESPONDENCE: Dr. Erik S.G. Stroes, Academic Medical Center, Department of Vascular Medicine, Room F4-211, P.O. Box 22660, 1100 DD, Amsterdam, the Netherlands. E-mail: e.s.stroes@amc.nl.

PERSPECTIVES

COMPETENCY IN MEDICAL KNOWLEDGE: Atherosclerosis is an inflammatory disease in which leukocytes are key cellular effectors. In addition to their involvement in early lesions, circulating leukocytes accumulate abundantly in advanced human atherosclerotic lesions.

TRANSLATIONAL OUTLOOK: As interventions that target leukocyte accumulation in atherosclerotic lesions undergo further investigation as a potential means of preventing ischemic events, SPECT/CT imaging may be a useful surrogate for efficacy.

REFERENCES

1. Nahrendorf M, Swirski FK. Monocyte and macrophage heterogeneity in the heart. Circ Res 2013;112:1624–33.

2. Weber C, Zernecke A, Libby P. The multifaceted contributions of leukocyte subsets to atherosclerosis: lessons from mouse models. Nat Rev Immunol 2008;8:802–15.

3. Galkina E, Ley K. Vascular adhesion molecules in atherosclerosis. Arterioscler Thromb Vasc Biol 2007;27:2292–301.

4. Ley K, Miller YI, Hedrick CC. Monocyte and macrophage dynamics during atherogenesis. Arterioscler Thromb Vasc Biol 2011;31:1506–16.

5. Dutta P, Courties G, Wei Y, et al. Myocardial infarction accelerates atherosclerosis. Nature 2012;487:325–9.

6. Leuschner F, Dutta P, Gorbatov R, et al. Therapeutic siRNA silencing in inflammatory monocytes in mice. Nat Biotechnol 2011;29:1005–10.

7. Okamoto M, Fuchigami M, Suzuki T, Watanabe N. A novel C-C chemokine receptor 2 antagonist prevents progression of albuminuria and atherosclerosis in mouse models. Biol Pharm Bull 2012;35:2069–74.

8. Peters W, Charo IF. Involvement of chemokine receptor 2 and its ligand, monocyte chemoattractant protein-1, in the development of atherosclerosis: lessons from knockout mice. Curr Opin Lipidol 2001;12:175–80.

9. Potteaux S, Gautier EL, Hutchison SB, et al. Suppressed monocyte recruitment drives macrophage removal from atherosclerotic plaques of Apoe-/- mice during disease regression. J Clin Invest 2011;121:2025–36.

10. Hansson GK, Hermansson A. The immune system in atherosclerosis. Nat Immunol 2011;12:204–12.

11. Zhou X, Robertson AK, Rudling M, Parini P, Hansson GK. Lesion development and response to immunization reveal a complex role for CD4 in atherosclerosis. Circ Res 2005;96:427–34.

12. Sabatine MS, Morrow DA, Cannon CP, et al. Relationship between baseline white blood cell count and degree of coronary artery disease and mortality in patients with acute coronary syndromes: a TACTICS-TIMI 18 (Treat Angina with Aggrastat and determine Cost of Therapy with an Invasive or Conservative Strategy- Thrombolysis in Myocardial Infarction 18 trial) substudy. J Am Coll Cardiol 2002;40:1761–8.

13. Rogacev KS, Cremers B, Zawada AM, et al. CD14++CD16+ monocytes independently predict cardiovascular events: a cohort study of 951 patients referred for elective coronary angiography. J Am Coll Cardiol 2012;60:1512–5.

14. Bekkering S, Joosten LA, van der Meer JW, Netea MG, Riksen NP. Trained innate immunity and atherosclerosis. Curr Opin Lipidol 2013;24:487–92.

15. Stenvinkel P, Karimi M, Johansson S, et al. Impact of inflammation on epigenetic DNA methylation - a novel risk factor for cardiovascular disease? J Intern Med 2007;261:488–99.

16. Wierda RJ, Geutskens SB, Jukema JW, Quax PH, van den Elsen PJ. Epigenetics in atherosclerosis and inflammation. J Cell Mol Med 2010;14:1225–40.

17. Wu C, Li F, Niu G, Chen X. PET imaging of inflammation biomarkers. Theranostics 2013;3:448–66.

18. Trivedi RA, Mallawarachi C, King-Im JM, et al. Identifying inflamed carotid plaques using in vivo USPIO-enhanced MR imaging to label plaque macrophages. Arterioscler Thromb Vasc Biol 2006;26:1601–6.

19. Herenius MM, Thurlings RM, Wijbrandts CA, et al. Monocyte migration to the synovium in rheumatoid arthritis patients treated with adalimumab. Ann Rheum Dis 2011;70:1160–2.

20. van Hemert FJ, Thurlings R, Dohmen SE, et al. Labeling of autologous monocytes with 99mTc-HMPAO at very high specific radioactivity. Nucl Med Biol 2007;34:933–8.

21. van RJ, Kroon J, Hoogenboezem M, et al. The Rho-guanine nucleotide exchange factor Trio controls leukocyte transendothelial migration by promoting docking structure formation. Mol Biol Cell 2012;23:2831–44.

22. Abeles RD, McPhail MJ, Sowter D, et al. CD14, CD16 and HLA-DR reliably identifies human monocytes and their subsets in the context of pathologically reduced HLA-DR expression by CD14(hi)/CD16(neg) monocytes: Expansion of CD14(hi)/CD16(pos) and contraction of CD14(lo)/CD16(pos) monocytes in acute liver failure. Cytometry A 2012;81:823–34.

23. Gower RM, Wu H, Foster GA, et al. CD11c/CD18 expression is upregulated on blood monocytes during hypertriglyceridemia and enhances adhesion to vascular cell adhesion molecule-1. Arterioscler Thromb Vasc Biol 2011;31:160–6.

24. Rudd JH, Myers KS, Bansilal S, et al. (18)Fluorodeoxyglucose positron emission tomography imaging of atherosclerotic plaque inflammation is highly reproducible: implications for atherosclerosis therapy trials. J Am Coll Cardiol 2007;50:892–6.

25. Duivenvoorden R, de GE, Elsen BM, et al. In vivo quantification of carotid artery wall dimensions: 3.0-Tesla MRI versus B-mode ultrasound imaging. Circ Cardiovasc Imaging 2009;2:235–42.

26. Rudd JH, Myers KS, Bansilal S, et al. Relationships among regional arterial inflammation, calcification, risk factors, and biomarkers: a prospective fluorodeoxyglucose positron-emission tomography/computed tomography imaging study. Circ Cardiovasc Imaging 2009;2:107–15.

27. Ye YX, Basse-Lusebrink TC, Arias-Loza PA, et al. Monitoring of monocyte recruitment in reperfused myocardial infarction with intramyocardial hemorrhage and microvascular obstruction by combined fluorine 19 and proton cardiac magnetic resonance imaging. Circulation 2013;128:1878–88.

28. Kircher MF, Grimm J, Swirski FK, et al. Noninvasive in vivo imaging of monocyte trafficking to atherosclerotic lesions. Circulation 2008;117:388–95.

29. Swirski FK, Pittet MJ, Kircher MF, et al. Monocyte accumulation in mouse atherogenesis is progressive and proportional to extent of disease. Proc Natl Acad Sci U S A 2006;103:10340–5.

30. Galkina E, Ley K. Leukocyte influx in atherosclerosis. Curr Drug Targets 2007;8:1239–48.

31. Yona S, Kim KW, Wolf Y, et al. Fate mapping reveals origins and dynamics of monocytes and tissue macrophages under homeostasis. Immunity 2013;38:79–91.

32. Libby P, Ridker PM, Hansson GK. Progress and challenges in translating the biology of atherosclerosis. Nature 2011;473:317–25.

33. Stoneman V, Braganza D, Figg N, et al. Monocyte/macrophage suppression in CD11b diphtheria toxin receptor transgenic mice differentially affects atherogenesis and established plaques. Circ Res 2007;100:884–93.

34. Robbins CS, Hilgendorf I, Weber GF, et al. Local proliferation dominates lesional macrophage accumulation in atherosclerosis. Nat Med 2013;19:1166–72.

35. Yla-Herttuala S, Bentzon JF, Daemen M, et al. Stabilization of atherosclerotic plaques: an update. Eur Heart J 2013;34:3251–8.

36. Kataoka Y, Shao M, Wolski K, et al. Myeloperoxidase levels predict accelerated progression of coronary atherosclerosis in diabetic patients: Insights from intravascular ultrasound. Atherosclerosis 2014;232:377–83.

37. Marnane M, Merwick A, Sheehan OC, et al. Carotid plaque inflammation on 18F-fluorodeoxyglucose positron emission tomography predicts early stroke recurrence. Ann Neurol 2012;71:709–18.

38. Menezes LJ, Kotze CW, Agu O, et al. Investigating vulnerable atheroma using combined (18)F-FDG PET/CT angiography of carotid plaque with immunohistochemical validation. J Nucl Med 2011;52:1698–703.

39. Ridker PM, MacFadyen J, Libby P, Glynn RJ. Relation of baseline high-sensitivity C-reactive protein level to cardiovascular outcomes with rosuvastatin in the Justification for Use of statins in Prevention: an Intervention Trial Evaluating Rosuvastatin (JUPITER). Am J Cardiol 2010;106:204–9.

40. Mosig S, Rennert K, Krause S, et al. Different functions of monocyte subsets in familial hypercholesterolemia: potential function of CD14+ CD16+ monocytes in detoxification of oxidized LDL. FASEB J 2009;23:866–74.

41. Cybulsky MI, Iiyama K, Li H, et al. A major role for VCAM-1, but not ICAM-1, in early atherosclerosis. J Clin Invest 2001;107:1255–62.

42. Combadiere C, Potteaux S, Rodero M, et al. Combined inhibition of CCL2, CX3CR1, and CCR5 abrogates Ly6C(hi) and Ly6C(lo) monocytosis and almost abolishes atherosclerosis in hypercholesterolemic mice. Circulation 2008;117:1649–57.

43. Tardif JC, McMurray JJ, Klug E, et al. Effects of succinobucol (AGI-1067) after an acute coronary syndrome: a randomised, double-blind, placebo-controlled trial. Lancet 2008;371:1761–8.

44. Kalinowska A, Losy J. Investigational C-C chemokine receptor 2 antagonists for the treatment of autoimmune diseases. Expert Opin Investig Drugs 2008;17:1267–79.

45. Weber C, Noels H. Atherosclerosis: current pathogenesis and therapeutic options. Nat Med 2011;17:1410–22.

KEY WORDS **atherosclerosis, imaging, inflammation, peripheral blood mononuclear cells**